ELSEVIER

Contents lists available at ScienceDirect

Ceramics International

journal homepage: www.elsevier.com/locate/ceramint



The effective role of akermanite on the apatite-forming ability of gelatin scaffold as a bone graft substitute



Azam Zare-Harofteh a, Samaneh Saber-Samandari b,*, Saeed Saber-Samandari c,*

- ^a Materials and Biomaterials Research Center, Tehran, Iran
- ^b Department of Chemistry, Eastern Mediterranean University, TRNC via Mersin 10, Gazimagusa, Turkey
- ^c New Technologies Research Center, Amirkabir University of Technology, Tehran, Iran

ARTICLE INFO

Article history:
Received 1 June 2016
Received in revised form
13 July 2016
Accepted 17 August 2016
Available online 18 August 2016

Keywords:
Bone tissue engineering
Scaffold
Bioactivity
Akermanite
Gelatin
Freeze-casting

ABSTRACT

When implanted in living body, a scaffold plays an important role in guiding new bone formation into desired shapes via the development of a biologically active, bone-like apatite layer on its surface. In this study, akermanite (Akr) nanoparticles were synthesized, and, using freeze-casting method, their different contents were applied in the preparation of porous gelatin (Gel) scaffolds. After, the nanocomposite scaffolds were immersed in a simulated body fluid (SBF) solution for 14 days, the bioactivity and apatite formation on their surfaces were examined. The prepared nanocomposite scaffolds before and after immersion in the SBF solution were characterized via the use of Fourier transform infrared (FTIR) spectroscopy, scanning electron microscopy (SEM), energy-dispersive X-ray spectroscopy (EDS), and X-ray diffraction (XRD) analysis. In addition, the elastic modulus and compressive strength of the scaffolds, as the candidate's mechanical properties, were investigated. According to the results, the prepared nanocomposite scaffolds with cellular and lamellar morphology exhibited preferentially and regularly oriented pores in the range of 94-125 um. Under optimum conditions, the Gel/Akr nanocomposite scaffolds with 93.5% swelling had a compressive strength of 1.1 MPa, an elastic modulus of 102 MPa. In addition, the in vitro bio-mineralization test confirmed that all samples were bioactive, and deposited apatite particles were detected with FTIR, XRD, SEM, and EDS after incubation in the SBF. The swelling ability of the scaffolds when immersed in water and phosphate buffer saline (PBS) was also investigated. The results of this study suggest that the prepared Gel/Akr nanocomposite scaffold that closely mimics the properties of bone tissue could be a promising biomedical material for clinical use in bone tissue engineering.

© 2016 Elsevier Ltd and Techna Group S.r.l. All rights reserved.

1. Introduction

In bone tissue engineering, scaffolds should be biocompatible, biodegradable, and mechanically robust. They should also facilitate early mineralization and support new bone formation while allowing for replacement with new bone [1,2]. Since bone consists of a porous composite of interpenetrating phases of collagen and hydroxyapatite, the scaffolds for bone regeneration should be similarly porous composites with interpenetrating polymer and ceramic phases [3].

It is not surprising that much research has been conducted on collagen and on its derivative Gel, since the organic matrix of bone is mainly collagen. Gel with a structural formula of NH₂COOH–CH–R, where R is amino acid of glycine, proline, and hydroxyl proline,

E-mail addresses: samaneh.saber@gmail.com (S. Saber-Samandari), saeedss@aut.ac.ir (S. Saber-Samandari).

is obtained by the thermal denaturation of collagen through the breaking of a triple-helix structure into random coils [4]. Since Gel is a denatured biopolymer, its selection as a scaffolding material can circumvent the concerns of immunogenicity and pathogen transmission that are associated with collagen [5]. Gel is also completely resorbable in vivo, and, compared to collagen, is easier to obtain in concentrated solutions [6,7]. For these reasons, Gel has been widely used in biomedical engineering as carriers for drug delivery [8], wound dressings [9], and scaffolds for bone tissue engineering [10]. Glutaraldehyde (GTA) has been clinically acceptable as a crosslinker of collagenous tissues in spite of its cytotoxicity [11]. Biocompatibility of the crosslinked scaffolds depend on the GTA concentration. Azami et al. claimed that the utilization of GTA as crosslinking agent in the concentration lower than 2.5% would not threaten cells' viability in the tissue engineering systems [12]. Nguyen et al. reported that the small amounts of GTA not only are shown to be nontoxic but also can increase the biocompatibility of cross-linked electro-spun Gel membranes [13]. Akermanite (Akr), a bioceramic having the structural formula of

^{*} Corresponding authors.

Ca₂MgSi₂O₇ and containing Si, Ca, and Mg, has received significant attention due to its more controllable mechanical properties and bioactivity [14]. It has been shown that Akr could improve cell stimulation and proliferation (i.e. adipose-derived [15] and osteoblasts [16]). In vitro and in vivo examinations suggest that Akr is more bioactive and thereby better stimulates the proliferation and differentiation of bone marrow-derived stem cells [17]. It also enhances, bone regeneration because of its superior biocompatibility and degradation [17]. Hence, Akr is an ideal candidate for bone tissue engineering [16].

In recent years, considerable attention has been given to the development of fabrication techniques to prepare porous ceramic scaffolds for bone tissue engineering. The ideal fabrication technique should produce 3D-shaped scaffolds with controlled porosity, shapes, and orientation in a reliable and economical way. Freeze-casting is a simple technique with which to produce porous, 3D-shaped ceramic or polymeric parts [18]. During this technique, ceramic slurry is poured into a mold and then frozen. The frozen solvent acts as a temporary binder to hold the part together for demolding. Subsequently, the part is subject to freezedrying to sublimate the solvent under vacuum, thus avoiding the drying stresses and shrinkage that may lead to cracks and warping during a normal drying process. After drying, the compacts are sintered in order to fabricate a porous material with improved strength and stiffness and the desired porosity. The result is a scaffold with a complex and often anisotropic porous microstructure that is generated during freezing [19].

To the best of our knowledge, the properties of a bioengineered nanocomposite scaffold based on Gel/Akr for bone tissue engineering have not previously been investigated. The aim of this study was to synthesis a novel bio-composite scaffold. The Gel/Akr nanocomposite scaffold was prepared with a combination of freeze-casting and freeze-drying methods. The scaffolds were carefully studied via structural (FTIR and XRD), morphological (SEM), and mechanical (Compressive Strength Test) analyses. The swelling ability of the scaffolds was investigated after immersion in water and in PBS. Finally, the bioactivity of prepared scaffolds was examined with the use of SBF.

2. Materials and methods

2.1. Materials

For the synthesis of Akr tetraethyl orthosilicate (Merck), magnesium nitrate hexahydrate (Merck), calcium nitrate tetrahydrate (Merck), and nitric acid (Merck) were used. Gel from porcine skin (microbiology grade, Aldrich) was used as received. GTA solution 25% in $\rm H_2O$ (Merck) was applied as a crosslinker. Sodium chloride, potassium chloride, sodium hydrogen carbonate, di-sodium hydrogen phosphate, magnesium chloride tetrahydrate, potassium dihydrogen phosphate, tris(hydroxymethyl) aminomethane, calcium chloride, and hydrochloric acid were purchased from Aldrich and were used for preparation of PBS and SBF solution.

2.2. Synthesis of nano-Akr powder

In this study, Akr powder was synthesized using sol-gel method [20]: 30 mL of tetraethyl orthosilicate ((C_2H_5O) $_4Si$, TEOS) was added to 30 mL of H_2O/HNO_3 mixture (with 2:1 mol ratio) and stirred for 30 min. Then, 15 g of magnesium nitrate hexahydrate ($Mg(NO_3)_2 \cdot 6H_2O$) and 30 g of calcium nitrate tetrahydrate ($C_4(NO_3)_2 \cdot 4H_2O$) were added into the above solution. The mol ratio of TEOS/ Mg^2+/Ca^2+ was 2:1:2. The reactants were continuously stirred for 5 h at room temperature. After that, the solution was kept in an oven at 60 °C for 24 h and then dried at 120 °C for 48 h.

The dried product was ground and sieved using 250-mesh, transferred into a crucible, and calcined at 1300 °C for 3 h. Finally, the powder was milled to find the nano-particles of Akr.

2.3. Fabrication of the nanocomposite scaffolds

First, the Gel was dissolved in deionized water (3% (w/v)) at 35 °C and stirred continuously for 1 h. Second, the different amounts of synthesized Akr (i.e., 10, 15, and 30% w/w of Gel) were added to the Gel solution and stirred vigorously for 2 h. The constant value of diluted GTA (1 wt%) solution was then added to the solution as a cross-linking agent and stirred again for 1 h. Following this step, the obtained well-dispersed slurries were poured into a polytetrafluoroethylene (PTFE) mold with a height of 20 mm and a diameter of 10 mm. The solution in the mold was freezecasted at -35 °C with a cooling rate of 1 °C/min for 35 min. The cooling rate was controlled by a proportional-integral-derivative (PID) controller using a ring heater and a thermocouple as liquid nitrogen was poured into the container. Next, the scaffolds' ice crystals were sublimated by the freeze dryer (FD-10, Pishtaz Engineering Co., Iran) at -55 °C for 48 h (see Scheme 1). Finally, the nanocomposite scaffolds (i.e., Gel/Akr-15, Gel/Akr-30, and Gel/Akr-50) with different contents of Akr were prepared. To minimize the residual GTA and to remove unreacted GTA, the prepared scaffolds were treated with aqueous solution of sodium borohydride (5%) for 3 h. Sodium borohydride as a reducing agent was used to block and convert the residual aldehyde to alcohol (hydroxyl groups) [21].

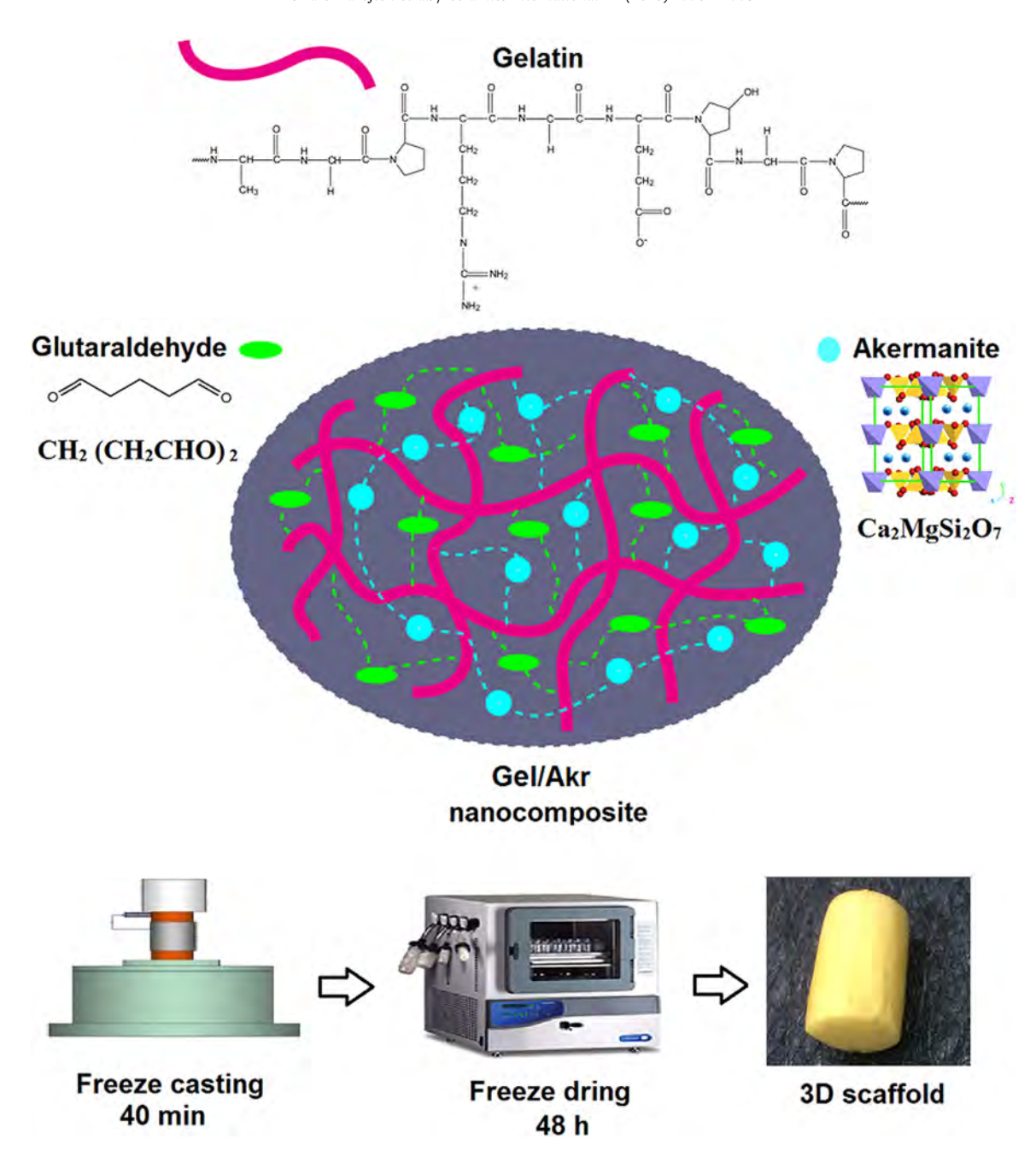
2.4. Release of glutaraldehyde

The release of excess and toxic GTA from the prepared scaffolds was evaluated by means of a spectrophotometric method [11]. The scaffolds were immersed in a PBS with pH of 7.4 at 37 $^{\circ}\text{C}$ for 24 h. After that, 10 mL of glycine solution (0.1 M) as an inactivator of GTA was added to the release buffer solution. The concentration of the released GTA in the solution was measured spectrophotometrically assayed using a UV–visible spectrophotometer (T80+UV/vis Spectrophotometer, Beijing PG Instrument Co., Ltd., China) at a wavelength of 436 nm and determined through comparison with a calibration curve.

It should be noted that the PBS solution was prepared by dissolving sodium chloride (8 g), potassium chloride (0.2 g), di-sodium hydrogen phosphate (1.44 g), and potassium di-hydrogen phosphate (0.24 g) in 800 mL of distilled water. After that, the pH of the solution was adjusted to 7.4 using a hydrochloric acid solution (1 mol L^{-1}). Finally, the volume of the solution reached 1 L by the addition of excess distilled water.

2.5. Characterization of the prepared nanocomposite scaffolds

The high-energy ball-milling operation was performed using a planetary ball mill (Retsch, PM400, Germany) in air at room temperature for 2 h. The milling speed was set at 300 rpm, and the ball-to-powder weight ratio was about 10:1. Zirconium oxide balls (50 mm in diameter), confined in a 500 mL bowl, and used as a milling medium. The size of the prepared and milled Akr powder was measured by dynamic light scattering (DLS) analysis, using a Malvern Zetasizer NanoZS 3600 (Malvern Instruments Limited, UK). FTIR spectra of samples were recorded using FTIR spectrometer (Perkin–Elmer, spectrum 400, USA) in the wavenumber range of 400–4000 cm⁻¹ using KBr pellets technique. SEM images of thin layer gold coated samples were taken by Stereoscan S360-Leica microscope (Cambridge, England). Energy-dispersive X-ray spectroscopy (EDS, Oxford instruments, UK) was applied to find the microstructure of the prepared nanocomposite scaffold before



 $\textbf{Scheme 1.} \ \ \textbf{The schematic illustration for synthesis of Gel/Ar nanocomposite scaffold.}$

and after apatite formation. A major phase of the prepared nanocomposite scaffolds were observed by X-ray difractometer (Unisantis, XMD 300, Germany) with a Cu-K α radiation (40 kV, 30 mA) over a 2θ range of $10-60^\circ$. In addition, mechanical properties of the prepared nanocomposite scaffolds were determined by compression strength test using a SANTAM (STM-20, Iran). The cylindrical samples with a diameter and height of 8 and 15 mm, respectively, were located between two compression plates, which was compressed with a 100 kN load cell and cross head speed of 0.2 mm/min. At least five specimens were tested for each sample.

2.6. Determination of porosity percentage and the pores size

The liquid replacement method was used to determine the porosity percentage of the prepared Akr/Gel nanocomposite scaffolds [22]. The prepared dried nanocomposite scaffold was

immersed in a gradual cylinder containing a known volume V_1 of water; after adding the scaffold, the volume of water was designated as V_2 . The new volume contained water and the dipped scaffold. After no more air bubbles were seen while keeping the scaffold under water, the scaffold was removed from the cylinder, and the volume of the cylinder (V_3), with water-filled pores, was reported. Finally, the volume of the scaffold was calculated by totaling the volume of water held by the scaffold ($V_1 - V_3$) and the volume of the prepared scaffolds ($V_2 - V_1$). The following equation was used to calculate the porosity percentage of the prepared scaffolds:

porosity(%) =
$$\frac{V_1 - V_3}{V_2 - V_3} \times 100$$
 (1)

In addition, the pore size of the prepared nanocomposite scaffolds was measured using ImageJ software. After selection five different cross-sectional SEM micrographs, the dimensions of more than 50 pores were measured and averaged to obtain a mean pore size.

2.7. Swelling behavior of the prepared nanocomposite scaffolds

The swelling behavior of the prepared nanocomposite scaffolds was explored by immersing of small pellets of the scaffolds (0.05 g) in 50 mL of either water or PBS solution at 37 °C. In different time intervals, the excess water on their surface was removed by a filter paper and the swollen scaffolds were weighed. Finally, the following equation was used to investigate the swelling percentage [23]:

Swelling(%) =
$$\frac{W_2 - W_1}{W_1} \times 100$$
 (2)

The weights of the swollen and the dried scaffold were W_2 and W_1 , respectively.

2.8. In vitro degradation of the prepared scaffolds

The biodegradation of the composites is an important factor, which influences the long-term functionality of the bone repairing or bone grafting [24]. For finding the degradation rate, the dried and weighed nanocomposite scaffolds with a diameter of 8 mm and height of 15 mm for each design were immersed in a 50 mL PBS at pH of 7.4 for 2 weeks and then incubated at 37 °C. The samples were removed at time intervals of 1, 3, 7, and 14 days, washed with distilled water, and dried in an oven at 50 °C for 24 h. Finally, degradation was calculated in terms of changes in the weight of the samples over the time period as shown in the following equation [25]:

$$Degradation(\%) = \frac{W_3 - W_1}{W_1} \times 100$$
 (3)

Where, W_1 is the initial mass of scaffolds and W_3 is the mass measured at a given time point.

2.9. In vitro evaluation of apatite forming ability

The bioactivity of the bone tissue engineering scaffolds contributes to their capability to form an apatite-like layer [26]. An SBF solution, prepared according to the procedure described by Kokubo and Takadama, was used to investigate the apatite-formation ability of the prepared Gel/Akr scaffolds [27]. Several reagent-grade salts (listed in Table 1) were dissolved in deionized water (800 mL) in a plastic beaker. The solution's pH was then adjusted to 7.25 by helping Tris and HCl solution (1 mol L^{-1}) at 37 °C.

The prepared Gel/Akr-30 nanocomposite scaffold was nominated for bioactivity evaluation according to its properties (e.g., porosity) close to the cancellous bone (this step is thoroughly explained in the next section). During the experiment, the scaffold (0.2 g) was immersed in 30 mL of SBF solution, which was refreshed every 3 days to maintain a pH of 7.4 at a temperature of 37 °C. After soaking for 3, 7, and 14 days, the samples were washed with deionized water and freeze-dried for 12 h. Finally, the surface morphology, chemical structure, and microstructure phase analysis of the prepared nanocomposite scaffolds were identified using SEM, EDS, FTIR and XRD analyses [17].

Table 1 lon concentrations of simulated body fluid and human blood plasma (mM).

	Na+	K+	Mg^{2+}	Ca ²⁺	Cl-	HCO ₃ -	HPO ₄ ²⁻	SO ₄ ²⁻
SBF Blood plasma			1.5 1.5		148.8 103.0		1.0 1.0	0.5 0.5

3. Results and discussion

3.1. Characterization of the prepared nanocomposite scaffolds

3.1.1. SEM analysis

Fig. 1 shows the morphology of the prepared nanocomposite scaffolds with different Akr contents in two different directions: perpendicular and cross-sections parallel to the direction of the ice front. As can be seen in the SEM images, the scaffolds have a lamellar structure, with long parallel pores aligned in the movement direction of the ice front. In addition, the honeycomb-like cross-sectional morphology contains preferential orientation and regular pores that are observed by controlling the growth direction of the ice crystals using the freeze-casting method. By directional freezing of the slurry, the particles in suspension are rejected from the moving ice front and are piled up between the growing columnar ice crystals [19]. Therefore, after the ice was freeze-dried and sublimated, pores with a negative replica the ice structure were created. These pores provide the rough texture on the sample surface, which is essential for cell attachment and proliferation.

Cancellous bone has 75-85% porosity, and its pores are 300-600 µm in diameter, which is a size much greater than that of cortical bone (5–10% porosity with pores that are 10–50 μm in diameter) [28]. Highly porous scaffolds fabricated from biomaterials have low degradation rates, possibly the result of a large surface area interacting with the host tissue, which can accelerate degradation due to macrophages via oxidation and/or hydrolysis. In contrast, the in vitro lower porosity of scaffolds with acceptable mechanical properties enhances osteogenesis due to cell aggregation and suppressed proliferation. Hulbert et al. determined that a minimum pore size of at least 100 µm is required for significant growth of bone cells in an implant [29]. Pore sizes and porosity of the samples were measured and tabulated (see Table 2). The porosity and average sizes of the interconnected pores for the prepared scaffolds varied in the range of 51-92% and 94-125 μm. By increasing the amounts of Akr nanoparticles in the scaffolds composition, the porosity increased, while the average pore size decreased due to increased crystallinity of the prepared grafted polymer nanocomposite scaffolds. As seen in Table 2, among the three prepared nanocomposite scaffolds, the Gel/Akr-30 sample has an adequate porosity of 77% and an average pore size of 110 µm, measurements which are close to those of cancellous bone. This can be caused by the numbers of Akr nanoparticles in the structure of the scaffold. Although, the smallest pore size of 94 µm was associated with the Gel/Akr-50 sample, this value is not appropriate for the growth of bone cells in a scaffold.

The EDS of the selected random place in the pore walls of the prepared nanocomposite scaffold (Gel/Akr-30) in Fig. 1 shows main signals for Gel (i.e., carbon, nitrogen, hydrogen, and oxygen) and Akr (i.e., calcium, magnesium, silicon, and oxygen), which their elements over the entire nanocomposites homogeneously distributed within the scaffolds [15].

3.1.2. Mechanical properties of the scaffolds

The scaffold should have adequate mechanical stability to provide a suitable environment for new bone tissue formation [30]. In its natural hydrated state, cortical bone has a compressive strength of 110–150 MPa and an elastic modulus of 18–22 GPa,

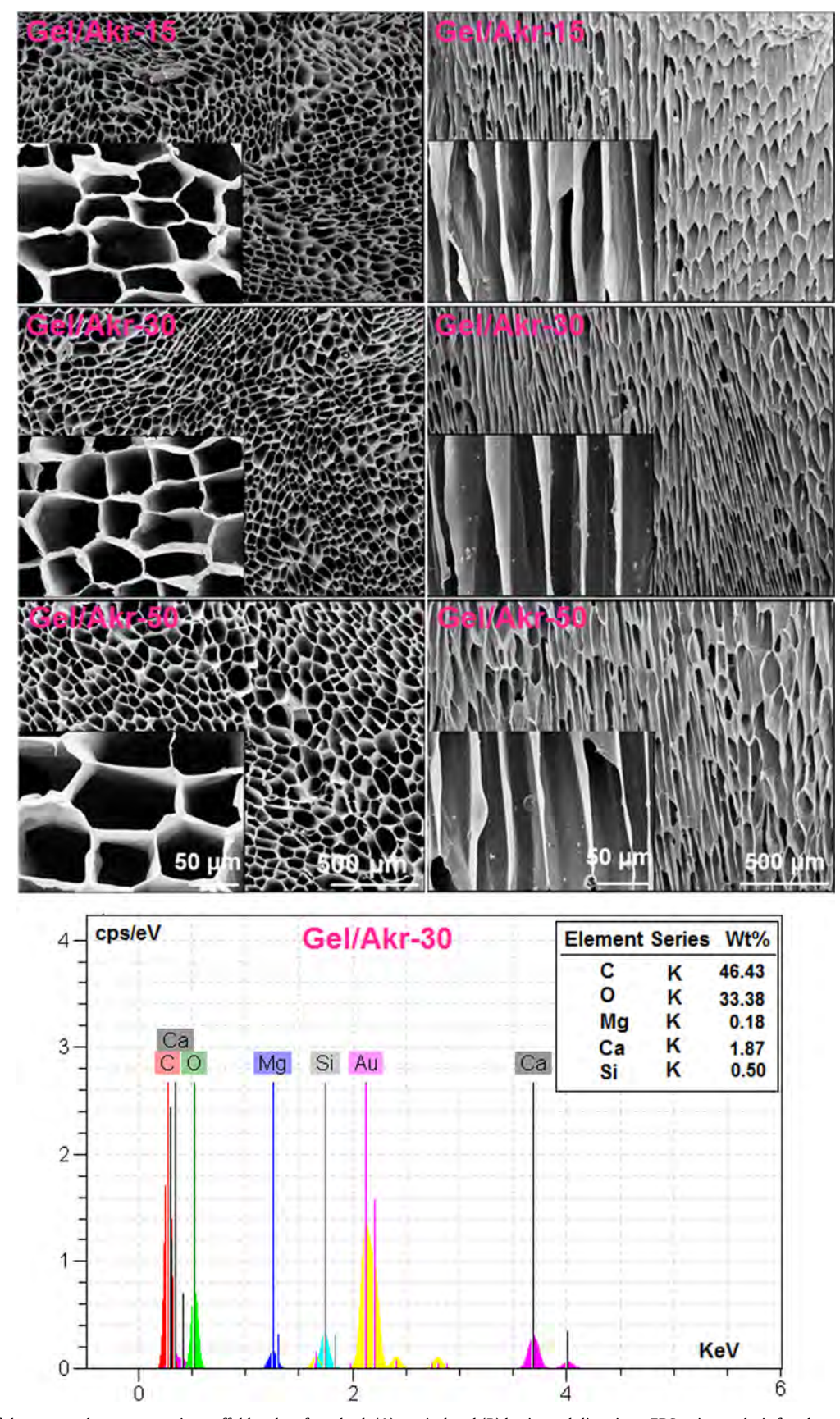


Fig. 1. SEM images of the prepared nanocomposite scaffolds taken from both (A) vertical and (B) horizontal directions, EDS point analysis for elemental composition of the prepared nanocomposite scaffold (Gel/Akr-30).

Table 2Average pore size, porosity, mechanical properties of the prepared nanocomposite scaffolds.

Sample	Pore size (µm)	Porosity (%)	Compressive strength (MPa)	Elastic modulus (MPa)	GTA re- lease (%)
Gel/Akr-15 Gel/Akr-30 Gel/Akr-50	110 ± 5	51 ± 3.3 77 ± 2.7 92 ± 2.5	$\begin{aligned} 1.4 \pm 0.090 \\ 1.1 \pm 0.075 \\ 0.98 \pm 0.080 \end{aligned}$	70 ± 5 102 ± 3 130 ± 8	0.31 0.58 0. 94

while cancellous bone has a compressive strength and an elastic modulus of 2-6 MPa and 0.1-0.3 GPa, respectively [28,31]. In general, the mechanical properties of prepared scaffolds can be affected by crystallinity, pore size, and porosity. A high level of crystallinity tends to increase the elastic modulus and the compressive strength. On the other hand, a large pore size or a high degree of porosity affects compressive strength only and tends to lower values. It is worth mentioning that an elastic modulus is an intrinsic property of a material. The compressive strength and the elastic modulus of the prepared nanocomposite scaffolds, which were calculated from the maximum point of the stress-strain curve and the slope of the initial linear portion of the stress-strain curve, are listed in Table 2. As was expected, increasing the Akr amount improved the elastic modulus of the nanocomposite scaffolds due to the increase in the ceramic phase. However, compressive strength depends on porosity. The results of this study revealed that Gel/Akr-50 has the highest degree of porosity and tends to lower the compressive strength of 0.98 MPa.

3.1.3. FTIR analysis

The FTIR spectrum of the prepared Gel/Akr-30 nanocomposite scaffold was compared with the spectra of pure Gel and the prepared Akr (see Fig. 2). The typical absorption bonds of the Gel situated at 1664 cm⁻¹ is attributed to the C=O stretching vibration of amide I. Amide II represents the bending vibrations of N–H groups and the stretching vibrations of C–N groups at 1544 cm⁻¹ and 1230 cm⁻¹, respectively. A peak related to aliphatic C–H bending vibrations was observed at 1450 cm⁻¹ [32]. Moreover, a broad peak, which was a distinguishing feature of the Gel, was assigned

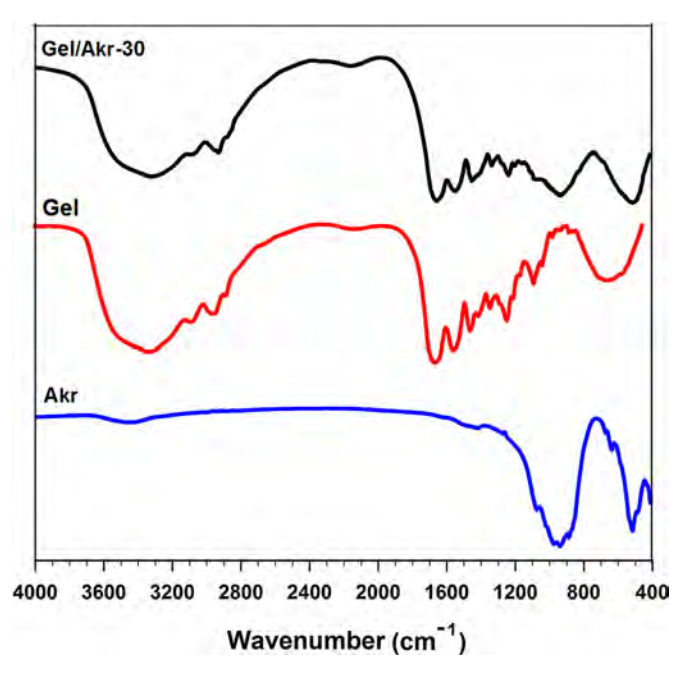


Fig. 2. Important peaks in FTIR spectra of Gel, Akr, and the prepared Gel/Akr-30 nanocomposite scaffold in the range of $400-4000~\rm cm^{-1}$.

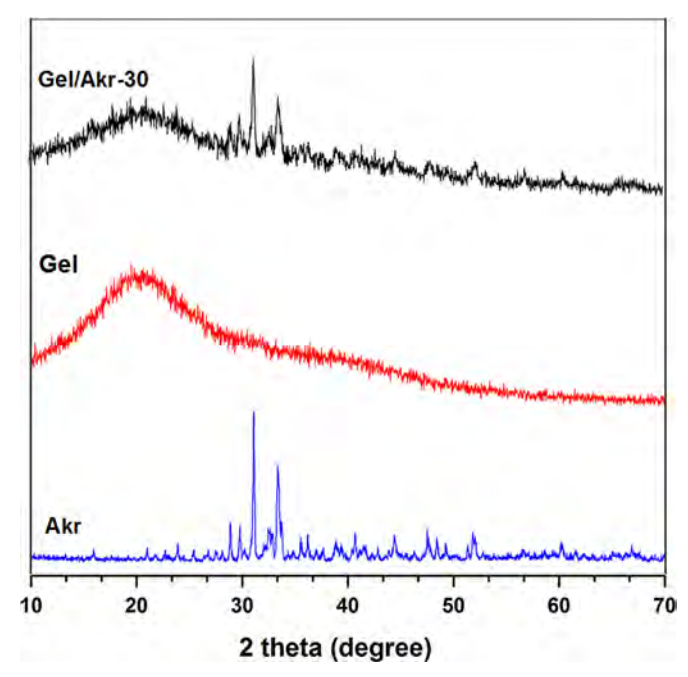


Fig. 3. XRD patterns of Gel, Akr, and the prepared Gel/Akr-30 nanocomposite scaffold.

to N–H stretching vibrations at 3300 cm⁻¹. In the spectrum of the prepared nanocomposite scaffold, all the characteristic peaks of the Gel seemed to be unchanged. However, some new peaks appeared which were related to the introduction of Akr in the Gel network. The FTIR spectrum of Akr contained the peaks assigned to the stretching vibrations O–Si–O bonds at 974 cm⁻¹, 935 cm⁻¹, and 852 cm⁻¹, which appeared as a cluster of peaks in the spectrum of the prepared nanocomposite scaffold. Other features of Akr were also found at 415 cm⁻¹ and 486 cm⁻¹ and correspond to the O–Ca–O and O–Mg–O bending modes, respectively. As seen in Fig. 2, the spectrum of the prepared nanocomposite scaffold was differentiated from the Gel spectrum by the presence of peaks in the mentioned ranges, which confirmed the presence of Akr, and consequently, electrostatic interactions between the Gel and the Akr.

3.1.4. XRD and DLS analysis

The XRD patterns of the prepared nanocomposite scaffold with the raw Gel and the prepared Akr are shown in Fig. 3. The XRD pattern of the prepared Akr was matched with the standard JCPDS pattern (96-900-6937) [33]. The crystallite size of the prepared Akr was calculated from the full width at half-maximum (FWHM) values via the use of Scherer's equation:

Crystallite size(L) =
$$\frac{K\lambda}{\beta\cos\theta}$$
 (4)

where λ is the X-ray wavelength, the parameter K is a constant related to the crystallite shape, which can be taken as 0.89 or 0.9. Theta (θ) is the Bragg angle, and β is the peak width of the diffraction peak profile at half maximum height, resulting from a small crystallite size in radians. The calculated crystallite size of Akr using this equation was found to be in the range of 90–150 nm, which is in agreement with the result of DLS analysis (see Fig. 4). According to the DLS analysis results, the synthesized Akr nanoparticles were found having diameters of 125.5 nm in a maximum mean volume (81% intensity) with narrow deviation and a single distribution.

In the nanocomposite scaffold pattern, the presence of Akr as the major phase and merwinite $(Ca_3MgSi_2O_8)$ and diopside

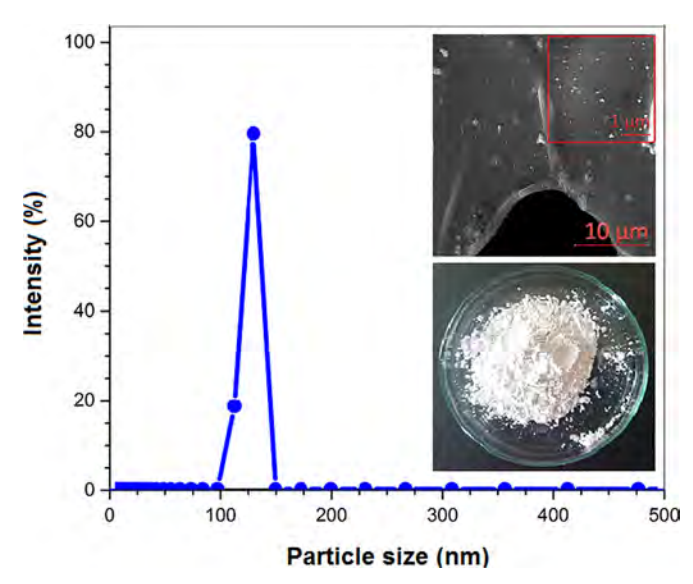


Fig. 4. The size distribution curve of the synthesized nanoparticles of Akr, insect shows the digital image of the synthesized Akr nanoparticles and the FESEM images of Gel/Akr-30 nanocomposite scaffold.

 $(\text{CaMgSi}_2\text{O}_6)$ as the minor phases was confirmed. In addition, the most intense broad peak related to the Gel at $2\theta\!=\!20$ appeared less intense in the pattern of the prepared nanocomposite scaffold. This decline in the intensity of the peak emphasizes the interactions between the Akr and Gel polymers. Based on the evidence obtained by FTIR, XRD, and EDS analyses, it can be concluded that the prepared scaffold is composed of Gel/Akr nanocomposites.

3.2. GTA release

Considering cytotoxic potential, the elimination of GTA from scaffold is of high significance [12]. A majority of the low concentrated GTA molecules in the crosslinked scaffold could react with Gel, where a minority of them that are unreacted residual GTA could quite easily washed off from the crosslinked scaffolds. In this study, the release of GTA from the prepared scaffolds was measured, while only the small amounts of GTA (1% w/v) were used and the prepared scaffolds were washed in order to remove poisonous unreacted GTA. As seen in Table 2, all the prepared scaffolds (i.e., Gel/Akr-15, 30 and 50) released very small amounts of GTA (less than 1%) after 24 h of immersion in PBS solution. Note that more unreacted GTA release was not found after immersion up to one week. This behavior is essential for biocompatible scaffolds as implants in bone tissue engineering.

3.3. Swelling behavior of the scaffolds

The swelling behavior and structural stability of implants are critical to their practical use in tissue engineering. The swelling capacity of the prepared nanocomposite scaffold (Gel/Akr-30) over 12 h of immersion in distilled water and PBS solution is shown in Fig. 5. First, the scaffold starts to uptake a large amount of solution very fast, and the rate of swelling increases. Throughout the time, significant differences in liquid uptake were not observed with further increases in time until the point at which a plateau was reached. This behavior can be described by the osmotic pressure difference between the scaffold and the solution [34]. The solution molecules were in contact with the surface of the scaffold, after which they attacked and penetrated the structure of the scaffold. This swelling behavior continued until the osmotic pressure difference between the solution and the scaffold was reduced as the result of an increase in water–scaffold interactions. Finally, the

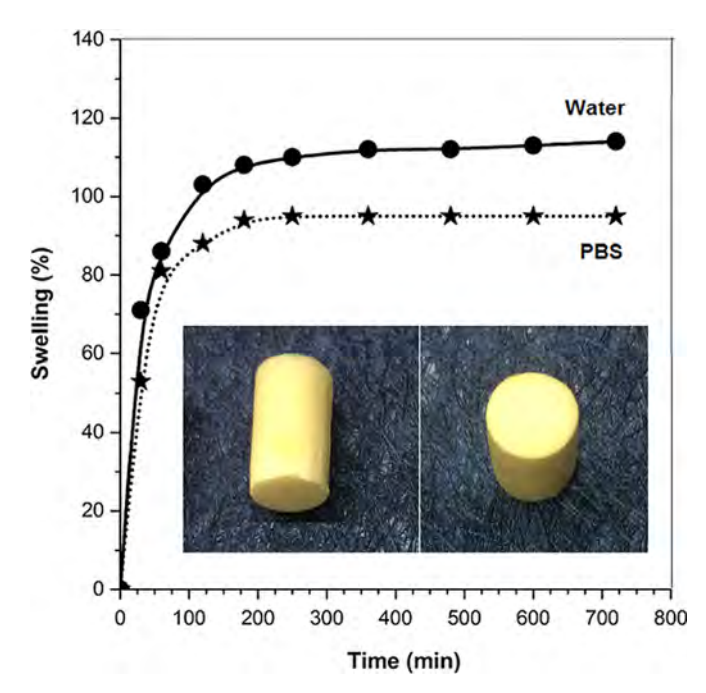


Fig. 5. Swelling behavior of the prepared nanocomposite scaffolds in distilled water and PBS solution, insect shows the digital image of the prepared nanocomposite scaffold (Gel/Akr-30).

osmotic forces were balanced, and a state of equilibrium in the scaffold swelling was achieved. The maximum swelling percentages of 114.3% and 93.5% were obtained using the Gel/Akr nanocomposite scaffold immersed in distilled water and PBS solution, respectively. As Fig. 5 illustrates, the water uptake ability of the scaffold decreased when placed in the PBS solution in comparison to that of distilled water, a finding that may be the result of the presence of Akr with the ionic crosslinking ability in the nanocomposite as a physical crosslinker [35]. The existence of Akr resulted in the generation of ionic interactions with the mono- and multivalent ions in the PBS solution. It thereby led to a decrease in the osmotic pressure difference between the scaffold and the external solution; and consequently, the water absorbency of the nanocomposite scaffold in the PBS solution was decreased [36,37].

3.4. In vitro degradation of scaffolds

Biodegradable scaffolds have a distinct advantage over non-biodegradable implants, as they provide the initial structure and stability for tissue formation, but degrade as the tissue forms, providing room for matrix deposition and tissue growth [26]. In this study, the prepared scaffolds were started to degrade after 3 days incubation. The weight loss was gradually increased with increasing soaking time. As shown in Fig. 6, the maximum degradation (18.9%) was found for Gel/Akr-50 sample with the highest amounts of Akr. Note that the degradation of scaffolds is highly dependent on their component dissolution. By the analysis of ionic products of Akr dissolution, the release of Si and Mg ions has confirmed its solubility in PBS solution [26,38]. Therefore, high solubility of Akr could be the main reason of more degradability of the Gel/Akr-50 sample.

3.5. In vitro bioactivity evaluation of the prepared nanocomposite scaffold

3.5.1. SEM analysis

To evaluate the formation of the apatite layer as an interface between the implant surface and the living bone tissue, the

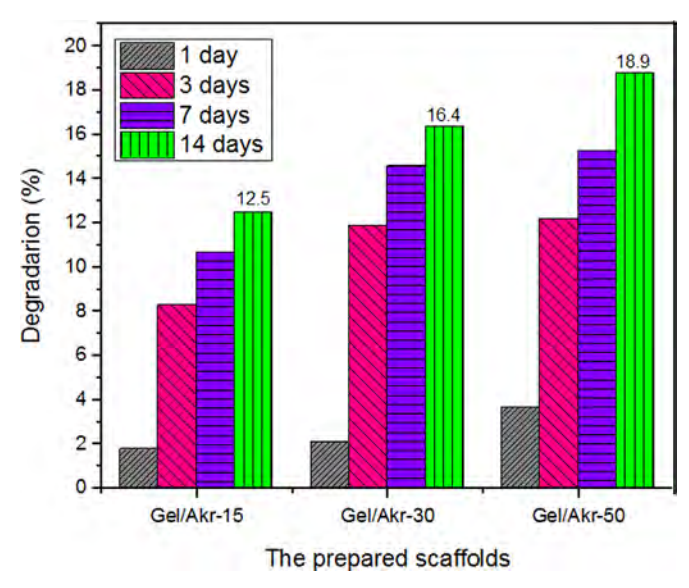


Fig. 6. Degradation behavior of the prepared nanocomposite scaffolds in PBS solution.

heterogeneous nucleation of apatite is essential from the SBF, which is a metastable calcium phosphate solution that is supersaturated with apatite. When the prepared scaffold containing Akr, like other silicate bioceramics (e.g., merwinite and diopside) is incubated in an SBF solution, a series of chemical reactions, such as spontaneous precipitation, nucleation, and growth of calcium phosphate, will cause an apatite layer to be formed. During the incubation period, hydronium ions (H₃O⁺) in the SBF solution were exchanged with cations on the surface of the scaffold, which leads to an increase in the solution's hydroxyl concentration. The mentioned negative hydroxyl ions of SBF react with the silica that is present in the composition of the scaffold. As a result, the silica hydrolysis, through breakage of the Si-O-Si bonds, rapidly leads to the formation of silanol (Si-OH) in the surface layer of the scaffold and finally stabilizes the pH of the SBF [33]. The silanol groups played the primary role in the apatite formation by inducing nucleation of the apatite by consuming calcium and phosphate ions from the SBF; therefore, the amorphous apatite-like layer will be formed on the prepared scaffold.

Fig. 7 shows the SEM images of the Gel/Akr-30 scaffold after soaking in SBF solution for 3, 7, and 14 days. After 3 days of soaking, a bone-like apatite layer starts to form on the surface of the scaffold. Once the layer of apatite nuclei are formed, they can grow spontaneously by consuming the calcium and phosphate ions present in the surrounding fluid; therefore, the rate of biomineralization was found to increase with a longer immersion period, and more apatite efficiently accumulated on the nanocomposite scaffold. As can be seen in Fig. 7, when the samples were soaked for 14 days, the apatite became more obvious, and the crystallite layers of apatite became more compact.

The random selection of an area in the pore wall of the prepared nanocomposite scaffold in the SEM image revealed the EDS spectrum. The result indicates the presence of calcium and phosphorus elements, which are attributed to the apatite phase of the bioactive scaffold.

3.5.2. FTIR analysis

Fig. 8 depicts the FTIR spectra of the prepared nanocomposite scaffold before and after incubation periods of 3, 7, and 14 days; all changes in the surface chemical composition of the scaffold are shown. The modifications that took place during the mineralization process were confirmed by the presence of three absorption

bands at 1092 cm⁻¹, 1029 cm⁻¹, and 961 cm⁻¹, which corresponds to the symmetric and asymmetric stretching modes of the phosphate groups (PO₄³⁻) in the hydroxyapatite [39,40]. In addition, the peaks attributed to some functional groups of Akr, such as Ca=O, O-Si-O, and Si-O, gradually decreased in relative intensities. Moreover, the peaks of O-Ca-O and O-Mg-O completely disappeared and were replaced by phosphate group peaks [33]. The two sharp peaks revealed at 560 and 602 cm⁻¹ were attributed to bending vibrations of the PO4³⁻ groups in the calcium phosphate crystalline phases [41]. Improvement in precision of the mentioned peak intensity by increasing the immersion time was solidly confirmed the formation of precipitated apatite layers on the surface of the scaffold.

3.5.3. XRD analysis

To investigate a deposition of apatite layer on the surface of the nanocomposite scaffold immersed in SBF solution for 3, 7, and 14 days, XRD analysis was performed; the results are shown in Fig. 9. As we explained in the previous study, the apatite's X-ray pattern shows crystalline peaks at $2\theta=23.2^{\circ}$, 26° , 29.3° , 32.2° , 46.6° , and 49.4° [42]. The prepared scaffold during the first three days of immersion in SBF exhibited the low intensity peaks related to the apatite. In fact, the very small amounts of apatite were precipitated, and the SBF solution during 3 days just changed the crystallinity of the scaffold compositions. After 7 days, the intensity of the apatite peaks, especially at $2\theta = 32.2$ and 46.6, was increased by extending the SBF soaking time. After 14 days, the surface was partly covered by an apatite layer, while, as shown in the XRD pattern, the Akr and Gel peaks completely disappeared. The results of this study confirmed the bioactivity of the prepared nanocomposite scaffold.

3.5.4. Mechanical properties

The mechanical properties of the prepared nanocomposite scaffolds after immersion in the SBF were examined and revealed no significant differences in compressive strength before (1.1 MPa) and after (1.4 MPa) immersion. However, the elastic modulus, which is an intrinsic property increased, from 102 MPa to 172 MPa when the sample was immersed in the SBF [43]. This could be due to the deposition of highly crystalline hydroxyapatite layers with an 18 ± 5 GPa elastic modulus on the surface of the scaffold [44].

4. Conclusion

The Gel/Akr nanocomposite scaffolds containing different volumes of the synthesized nanoparticles of Akr were prepared via a freeze-casting method. The prepared scaffolds were characterized by FTIR, XRD, SEM, and EDS. The results confirmed that by increasing the volume of Akr nanoparticles in the structure of scaffolds, the pore size decreased while the porosity percentage increased. The elastic modulus and compressive strength were increased by increasing the amounts of Akr. The maximum swelling percentages of the Gel/Akr nanocomposite scaffold were 114.3% and 93.5% after immersion in distilled water and PBS solution, respectively. The water uptake ability of the scaffold decreased when placed in the PBS solution in comparison to that of distilled water. To evaluate the bioactivity and the apatite-forming ability of the scaffolds, a sample was soaked in SBF for 3, 7, and 14 days. The results revealed that the prepared scaffold possessed apatiteforming ability in SBF. The apatite particles were well deposited on the surface of the scaffold, whereas the formed crystallites played an essential role in the formation, growth, and maintenance of the tissue-biomaterials interface. Thus, the results suggest that the synthesized Gel/Akr scaffold is a potential candidate material to use in bone tissue engineering.

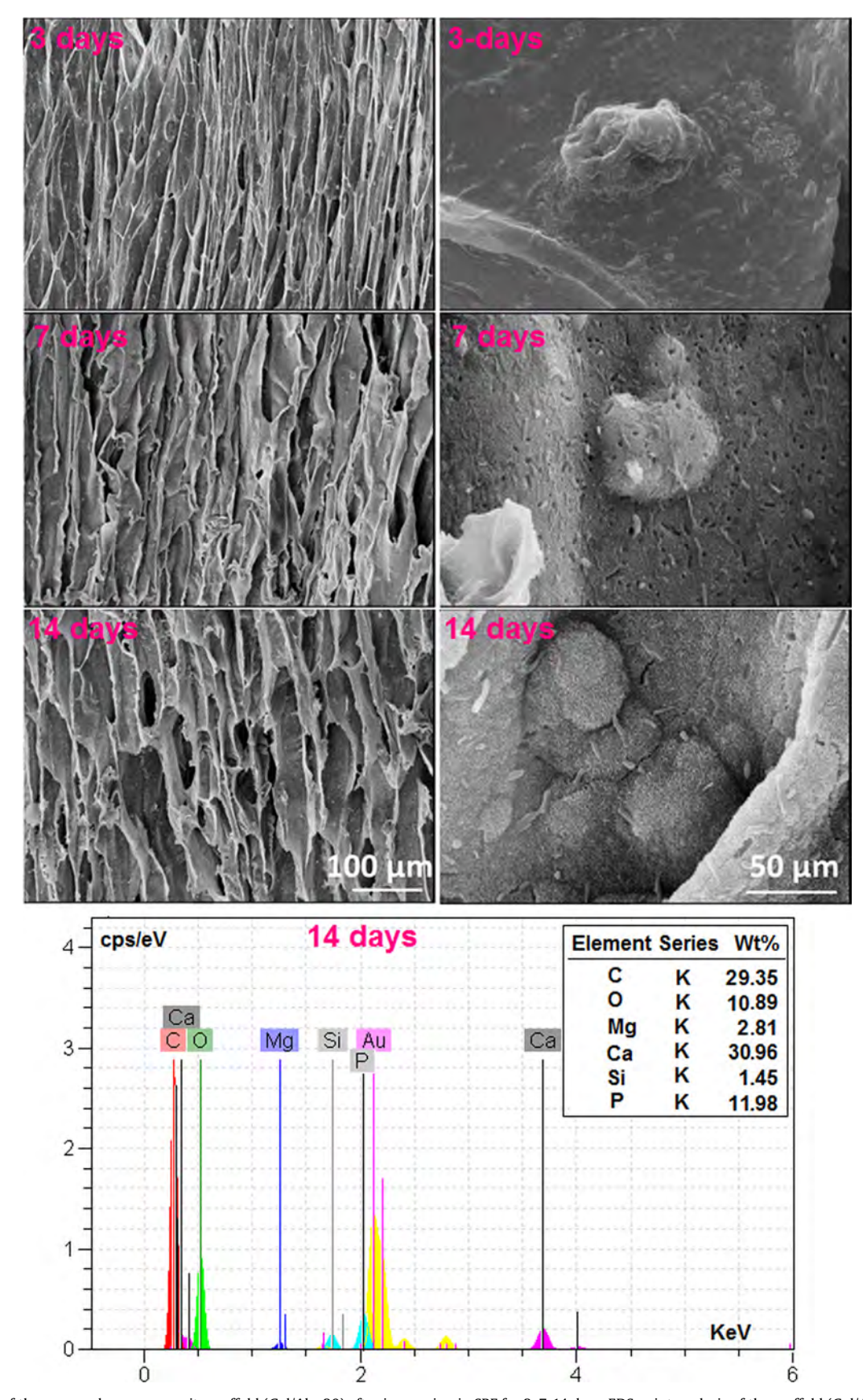


Fig. 7. SEM image of the prepared nanocomposite scaffold (Gel/Akr-30) after immersion in SBF for 3, 7, 14 days, EDS point analysis of the scaffold (Gel/Akr-30) after 14 days immersion in SBF.

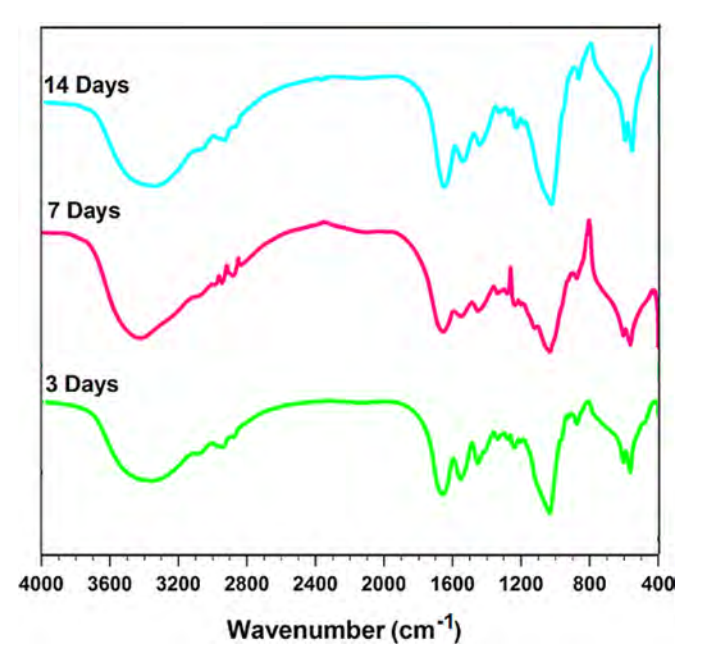


Fig. 8. Important peaks in FTIR spectra of the prepared nanocomposite scaffold (Gel/Akr-30) before and after soaking in SBF for 3, 7 and 14 days in the range of $400-4000~\rm cm^{-1}$.

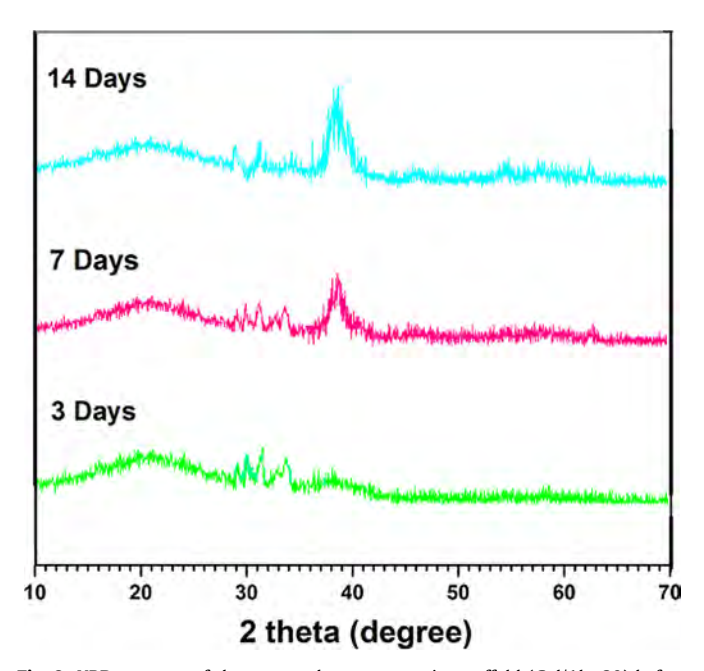


Fig. 9. XRD patterns of the prepared nanocomposite scaffold (Gel/Akr-30) before and after soaking in SBF for 3, 7 and 14 days.

Acknowledgment

This research was partially supported by the New Technologies Research Center. We thank Dr. Ali Zamanian from the Materials and Energy Research Center who provided insight and expertize that greatly assisted the research.

References

- J. Li, H. Sun, D. Sun, Y. Yao, F. Yao, K. Yao, Biomimetic multicomponent polysaccharide/nano-hydroxyapatite composites for bone tissue engineering, Carbohydr. Polym. 85 (2011) 885–894.
- [2] Y. Tang, K. Zhao, L. Hu, Z. Wu, Two-step freeze casting fabrication of

- hydroxyapatite porous scaffolds with bionic bone graded structure, Ceram. Int. 39 (2013) 9703–9707.
- [3] A. OLad, F. Arshi Azhar, The synergetic effect of bioactive ceramic and nanoclay on the properties of chitosan–gelatin/nanohydroxyapatite–montmorillonite scaffold for bone tissue engineering, Ceram. Int. 40 (2014) 10061–10072.
- [4] A. Veis, The Macromolecular Chemistry of Gelatin, Academic Press, New York, 1964
- [5] X. Liu, L.A. Smith, J. Hu, P.X. Ma, Biomimetic nanofibrous gelatin/apatite composite scaffolds for bone tissue engineering, Biomaterials 30 (2009) 2252–2258.
- [6] P.I. Rose, Gelatin Wiley, New York, 1987.
- [7] A. Bigi, S. Panzavolta, K. Rubini, Relationship between triple-helix content and mechanical properties of gelatin films, Biomaterials 25 (2004) 5675–5680.
- [8] H.C. Liang, W.H. Chang, K.J. Lin, H.W. Sung, Genipin-crosslinked gelatin microspheres as a drug carrier for intramuscular administration: in vitro and in vivo studies, J. Biomed. Mater. Res. 65 (2003) 271–282.
- [9] W.H. Chang, Y. Chang, P.H. Lai, H.W. Sung, A genipin-crosslinked gelatin membrane as wound-dressing material: in vitro and in vivo studies, J. Biomater. Sci. Polym. 14 (2003) 481–495.
- [10] X. Wu, Y. Liu, X. Li, P. Wen, Y. Zhang, Y. Long, X. Wang, Y. Guo, F. Xing, J. Gao, Preparation of aligned porous gelatin scaffolds by unidirectional freeze-drying method, Acta Biomater. 6 (2010) 1167–1177.
- [11] A. Bigi, G. Cojazzi, S. Panzavolta, K. Rubini, N. Roveri, Mechanical and thermal properties of gelatin flms at different degrees of glutaraldehyde crosslinking, Biomaterials 22 (2001) 763–768.
- [12] M. Azami, M. Rabiee, F. Moztarzadeh, Glutaraldehyde crosslinked gelatin/hy-droxyapatite nanocomposite scaffold, engineered via compound techniques, Polym. Compos. 31 (2010) 2112–2120.
- [13] T.H. Nguyen, B.T. Lee, Fabrication and characterization of cross-linked gelatin electro-spun nano-fibers. I. Biomed. Sci. Eng. 3 (2010) 1117–1124.
- electro-spun nano-fibers, J. Biomed. Sci. Eng. 3 (2010) 1117–1124.
 [14] H. Gu, F. Guo, X. Zhou, L. Gong, Y. Zhang, W. Zhai, L. Chen, L. Cen, S. Yin, J. Chang, L. Cui, The stimulation of osteogenic differentiation of human adipose-derived stem cells by ionic products from akermanite dissolution via activation of the ERK pathway, Biomaterials 32 (2011) 7023–7033.
- [15] F. Karkeh-abadi, S. Saber-Samandari, S. Saber-Samandari, The impact of functionalized CNT in the network of sodium alginate-based nanocomposite beads on the removal of Co(II) ions from aqueous solutions, J. Hazard. Mater. 312 (2016) 224–233.
- [16] C. Wu, J. Chang, S. Ni, J. Wang, In vitro bioactivity of akermanite ceramics, J. Biomed. Mater. Res. 76 (2006) 73–80.
- [17] S. Saber-Samandari, S. Saber-Samandari, F. Ghonjizade-Samani, J. Aghazadeh, A. Sadeghi, Bioactivity evaluation of novel nanocomposite scaffolds for bone tissue engineering: The impact of hydroxyapatite, Ceram. Int. 42 (2016) 11055–11062.
- [18] T. Fukasawa, Z.Y. Deng, M. Ando, T. Ohji, Y. Goto, Pore structure of porous ceramics synthesized from water-based slurry by freeze-dry process, J. Mater. Sci. 36 (2001) 2523–2527.
- [19] S. Deville, E. Saiz, A.P. Tomsia, Freeze casting of hydroxyapatite scaffolds for bone tissue engineering, Biomaterials 27 (2006) 5480–5489.
- [20] C. Wu, J. Chang, Synthesis and apatite-formation ability of akermanite, Mater. Lett. 58 (2004) 2415–2417.
- [21] H. Jiankang, L. Dichen, L. Yaxiong, Y. Bo, L. Bingheng, L. Qin, Fabrication and characterization of chitosan/gelatin porous scaffolds with predefined internal microstructures, Polymer 48 (2007) 4578–4588.
- [22] S. Saber-Samandari, S. Saber-Samandari, S. Kiyazar, J. Aghazadeh, A. Sadeghi, In vitro evaluation for apatite-forming ability of cellulose-based nanocomposite scaffolds for bone tissue engineering, Int. J. Biol. Macromol. 86 (2016) 434–442.
- [23] S. Saber-Samandari, H.O. Gulcan, S. Saber-Samandari, M. Gazi, Efficient removal of anionic and cationic dyes from an aqueous solution using pullulangraft-polyacrylamide porous hydrogel, Water Air Soil Pollut. 225 (2014) 2177.
- [24] A. Shavandi, A.E.A. Bekhit, M.A. Ali, Z. Sun, M. Gould, Development and characterization of hydroxyapatite/β-TCP/chitosan composites for tissue engineering applications, Mater. Sci. Eng. C 56 (2015) 481–493.
- [25] C.G. Jeong, S.J. Hollister, Mechanical, permeability, and degradation properties of 3D designed Poly(1,8 octanediol-co-citrate) scaffolds for soft tissue engineering, J. Biomed. Mater. Res. B Appl. Biomater. 93 (2009) 141–149.
- [26] C. Wu, J. Chang, W. Zhai, S. Ni, J. Wang, Porous akermanite scaffolds for bone tissue engineering: preparation, characterization, and in vitro studies, J. Biomed Mater. Res. B. Appl. Biomeder. 78B (2006) 47, 55
- Biomed. Mater. Res. B Appl. Biomater. 78B (2006) 47–55. [27] T. Kokubo, H. Takadama, How useful is SBF in predicting in vivo bone bioactivity? Biomaterials 27 (2006) 2907–2915.
- [28] S. Lee, M. Porter, S. Wasko, G. Lau, P.Y. Chen, E.E. Novitskaya, A.P. To msia, A. Almutairi, M.A. Meyers, J. McKittrick, Potential bone replacement materials prepared by two methods, Mater. Res. Soc. Symp. Proc. 1418 (2012) 177–181.
- [29] S.F. Hulbert, F.A. Young, R.S. Mathews, J.J. Klawitter, C.D. Talbert, F.H. Stelling, Potential of ceramic materials as permanently implantable skeletal prostheses, J. Biomed. Mater. Res. 4 (1970) 433–456.
- [30] X. Liu, P.X. Ma, Polymeric scaffolds for bone tissue engineering, Ann. Biomed. Eng. 32 (2004) 477–486.
- [31] P.Y. Chen, J. McKittrick, Compressive mechanical properties of demineralized and deproteinized cancellous bone, J. Mech. Behav. Biomed. Mater. 4 (2011) 961–973
- [32] C. Zhuang, F. Tao, Y. Cui, Anti-degradation gelatin films crosslinked by active ester based on cellulose, RSC Adv. 5 (2015) 52183–52193.
- [33] R. Choudhary, S. Koppala, S. Swamiappan, Bioactivity studies of calcium

- magnesium silicate prepared from eggshell waste by sol–gel combustion synthesis, J. Asian Ceram. Soc. 3 (2015) 173–177.
- [34] S. Saber-Samandari, O. Yilmaz, E. Yilmaz, Photoinduced graft copolymerization onto chitosan under heterogeneous conditions, J. Macromol. Sci. A 49 (2012) 591–598.
- [35] S. Saber-Samandari, S. Saber-Samandari, S. Heydaripour, M. Abdouss, Novel carboxymethyl cellulose based nanocomposite membrane: synthesis, characterization and application in water treatment, J. Environ. Manag. 166 (2016) 457–465.
- [36] S. Saber-Samandari, M. Gazi, O. Yilmaz, Synthesis and characterization of chitosan-graft-poly(*n*-allyl maleamic acid) hydrogel membrane, Water Air Soil Pollut. 224 (2013) 1624.
- [37] H. Hosseinzadeh, S. Mohammadi, Quince seed mucilage magnetic nanocomposites as novel bioadsorbents for efficient removal of cationic dyes from aqueous solutions, Carbohydr. Polym. 134 (2015) 213–221.
- [38] L. Xia, Z. Zhang, L. Chen, W. Zhang, D. Zeng, X. Zhang, J. Chang, X. Jiang, Proliferation and osteogenic differentiation of human periodontal ligament cells on akermanite and β -TCP bioceramics, Eur. Cell Mater. 22 (2011) 68–82.

- [39] S. Saber-Samandari, S. Saber-Samandari, M. Gazi, F.C. Cebeci, E. Talasaz, Synthesis, characterization and application of cellulose based nano-biocomposite hydrogels, J. Macromol. Sci. Pure Appl. Chem. 50 (2013) 1133–1141.
- [40] J.P. Lafon, E. Champion, D. Bernache-Assollant, R. Gibert, A.M. Danna, Thermal decomposition of carbonated calcium phosphate apatites, J. Therm. Anal. Calorim. 72 (2003) 1127–1134.
- [41] S. Saber-Samandari, K. Alamara, S. Saber-Samandari, K.A. Gross, Micro-Raman spectroscopy shows how the coating process affects the characteristics of hydroxylapatite, Acta Biomater. 9 (2013) 9538–9546.
- [42] S. Saber-Samandari, N. Nezafati, S. Saber-Samandari, The effective role of hydroxyapatite-based composites in anticancer drug-delivery systems, Crit. Rev. Ther. Drug 33 (2016) 41–75.
- [43] J. Adamcik, C. Lara, I. Usov, J.S. Jeong, F.S. Ruggeri, G. Dietler, H.A. Lashuel, I. W. Hamley, R. Mezzenga, Measurement of intrinsic properties of amyloid fibrils by the peak force QNM method, Nanoscale 4 (2012) 4426–4429.
- [44] S. Saber-Samandari, C.C. Berndt, K.A. Gross, Selection of the implant and coating materials for optimized performance by means of nanoindentation, Acta Biomater. 7 (2011) 874–881.